

Diversity of coherences and origin of electronic transitions of supermolecular nanoring

Vytautas Butkus,^{1,2,*} Jan Alster,^{3,†} Eglė Bašinskaitė,¹ Ramūnas Augulis,^{3,‡} Patrik Neuhaus,⁴ Leonas Valkunas,^{1,2} Harry L. Anderson,⁴ Darius Abramavicius,¹ and Donatas Zigmantas^{3,§}

¹*Department of Theoretical Physics, Faculty of Physics, Vilnius University, Sauletekio Avenue 9-III, 10222 Vilnius, Lithuania*

²*Center for Physical Sciences and Technology, Savanoriu Avenue 231, 02300 Vilnius, Lithuania*

³*Department of Chemical Physics, Lund University, P.O. Box 124, SE-22100 Lund, Sweden*

⁴*Department of Chemistry, University of Oxford, Chemistry Research Laboratory, Mansfield Road, Oxford OX1 3TA, United Kingdom*

Quantum coherence is highly involved in photochemical functioning of complex molecular systems. Co-existence and intermixing of electronic and/or vibrational coherences, while never unambiguously identified experimentally, has been proposed to be responsible for this phenomenon. Analysis of multidimensional spectra of a synthetic belt-shaped molecular six-porphyrin nanoring with an inner template clearly shows a great diversity of separable electronic, vibrational and mixed coherences and their cooperation shaping the optical response. The results yield clear assignment of electronic and vibronic states, estimation of excitation transfer rates, and decoherence times. Theoretical considerations prove that the complexity of excitation dynamics and spectral features of the nanoring excitation spectrum is due to combined effect of cyclic symmetry, small geometrical deformations, and vibronic coupling.

Electronic energy transfer (EET) in organic polymers plays a central role in their versatile applications as electric charge carrying or light emitting/absorbing moieties, allowing facile and cheap production of optoelectronic devices[1]. Even though various nanomaterials, including quantum dots or carbon nanotubes, have been extensively studied, the interest still persists due to the great variability of their optical and electronic properties and enormous chemical diversity.

EET in large supra-molecular systems is necessarily related to coherent phenomena, arising from the quantum mechanical nature of the inner microscopic constituents. In the conditions of electronic–vibrational resonance, quantum mixing of electronic and nuclear degrees of freedom of vibronically coupled molecular systems were suggested to result in a host of phenomena beyond the adiabatic approximation[2, 3].

Recent development of ultrafast nonlinear spectroscopic techniques, such as the two-dimensional electronic spectroscopy (2DES) facilitated direct observation of quantum superpositions in the form of quantum beats (dynamic coherences)[4–10]. Although 2DES combines correlation information between excitation and detection frequencies and simultaneously ensures high spectral and temporal resolutions, the experimental identification of coherences and determination of their origin is a very complex issue. The questionable nature of the long-lived dynamic coherences in the iconic

Fenna–Matthews–Olson (FMO) light-harvesting complex (whether electronic[4] or vibrational[2, 11, 12]) still causes debates. Mechanisms related to electronic–vibrational mixing[13, 14], inter-pigment correlations[15], non-secular quantum transport[16], and inhomogeneous broadening[17] were proposed to be important, allowing FMO to maintain the dynamic quantum coherence for as long as a few picoseconds.

The role of electronic–vibrational mixing in molecular systems is of a particular interest, since it was recently shown that diabatic coupling to coherent vibrational modes might enhance the rate of EET[14, 18, 19] and of the charge transfer[9, 10]. However, this implies existence of both electronic and vibrational coherences in the same system at the same time, what has never been unambiguously observed.

Porphyrin nanoring, the chemical structure of which is depicted in Fig. 1A, was chosen for this quest. It consists of six zinc(II) porphyrin molecules forming a belt around an inner hexapyridyl template; the porphyrins contain aryl groups (3,5-di(tri-hexylsilane)benzene) at meso-positions and are interconnected by acetylenes. The fine structure of the peaks identified as S_1 through S_6 in its absorption spectrum at 77K (Fig. 1B) suggests that coherences in 2DES might be clearly resolvable for this system.

Previous quantum chemistry calculations using the time-dependent density functional theory estimated the lowest-energy S_0 – S_1 transition to be around 10566 cm^{-1} . The sequence of almost equally-spaced strong peaks (for the nanoring studied here found at 11655 cm^{-1} , 12295 cm^{-1} and 12862 cm^{-1}) were discussed to stem from the Franck–Condon progression of the vibrational $\sim 605\text{ cm}^{-1}$ mode [20].

Two separate 2DES measurements of the fully conjugated porphyrin hexamer nanoring were performed at 77 K using laser pulses, the spectrum of which was cen-

* These authors equally contributed to this work

† These authors equally contributed to this work ; Current address: Faculty of Mathematics and Physics, Charles University in Prague, Ke Karlovu 3, 121 16 Prague, Czech Republic

‡ Current address: Center for Physical Sciences and Technology, Savanoriu Avenue 231, 02300 Vilnius, Lithuania

§ donatas.zigmantas@chemphys.lu.se

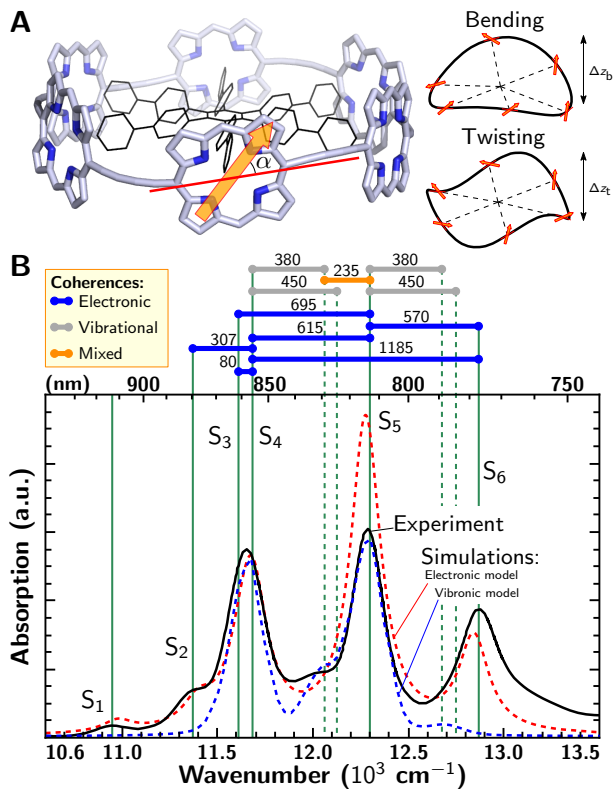


Figure 1. **Structure (A) and absorption spectrum (B) of the porphyrin nanoring.** Deformations used in the excitonic calculation are shown on the right. (B) Measured (black solid line) and simulated (red and blue dashed lines) absorption spectrum at 77 K. Energies of the electronic transitions to states $S_1 - S_6$ are indicated by solid vertical lines; vibronic transitions are indicated by vertical dashed lines. Frequencies of resolved coherent beatings are shown as colored segments, connecting the states involved in the corresponding quantum superpositions.

tered either at 800 nm or at 880 nm, thus covering different parts of the absorption spectrum (refer to the upper panels in Fig. 2A-B for the corresponding laser spectra). Refer to the Supplementary Materials and Methods section.

The 2D spectrum obtained using laser pulses at 880 nm covers the lowest electronic transition (Fig. 2A). It is dominated by a strong diagonal peak at $\sim 11655 \text{ cm}^{-1}$. Other features on the diagonal, related to the absorption peaks at 10941 cm^{-1} (S_1) and 11373 cm^{-1} (S_2), are much weaker. However, the peaks above the diagonal (“ P_{12} ”, “ P_{13} ” and “ P_{23} ”) connecting the three diagonal peaks can be clearly resolved in Fig. 2A. Excited state absorption shows up as strong negative features below the diagonal overlapping with positive peaks.

Laser pulses with the spectrum centered at 800 nm were used to investigate the spectral range of the other three most prominent transitions. The corresponding 2D spectrum is shown in Fig. 2B. The spectrum is very rich in features and at least 17 peaks can be clearly resolved. Interestingly, a peak on the diagonal at around

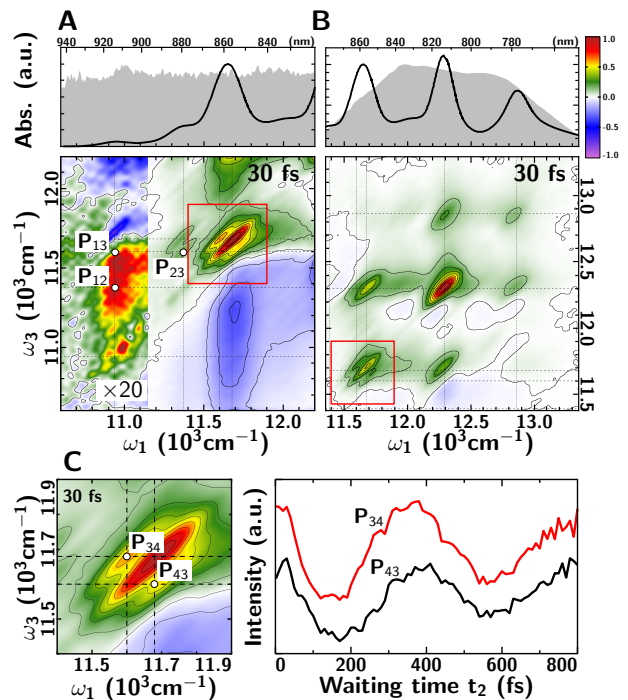


Figure 2. **The absorptive two-dimensional spectra at different excitation conditions and at 30 fs of the waiting time.** Spectra were obtained using laser pulses centered at 880 nm (A) and at 800 nm (B), respectively. In the upper panels, laser pulse and nanoring absorption spectra are shown. In (A) the signal value is multiplied by a factor of 20 for the plot range where $\omega_1 < 11157 \text{ cm}^{-1}$. (C) Zoomed in region of a degenerate peak in the 800 nm measurement (shown by red squares in (A) and (B)) and oscillatory dynamics of the “ P_{34} ” and “ P_{43} ” peaks. Spectra are drawn using linear colour scale, normalized to the maximum of each spectrum. Dashed vertical and horizontal lines indicate the energies of states $S_1 - S_6$.

11655 cm^{-1} consists of two previously not resolved[20, 21] contributions separated by $\sim 80 \text{ cm}^{-1}$. It could be estimated from the position of the off-diagonal peaks, indicated as P_{34} and P_{43} in Fig. 2C that the energies corresponding to these states are around 11600 cm^{-1} (S_3) and 11680 cm^{-1} (S_4).

To determine the energy dynamics via the manifold of excited states, the 2DES data were taken as a function of the waiting time t_2 , thus, making the complete 3D spectrum. Feature-rich oscillatory evolution has been observed throughout the whole (ω_1, ω_3) 2D area as a function of t_2 . Decaying dynamics was extracted using three-exponential-decay fitting with one variable time constant of 156–250 fs and remaining lifetimes of 235 ps and $\gg 1$ ns. The shortest timescale is related to the downward energy relaxation in the exciton manifold. This process is observed as the decay of the peaks on the diagonal of the spectrum and simultaneous increase of the peaks away from the diagonal if no other competing channel exists[22, 23]. The longer timescales represent the relaxation from the lowest state of the exciton manifold to the

Table I. **Classification of the observed coherences** ($<700 \text{ cm}^{-1}$). Average of four separate measurements are considered and the extracted dephasing times and standard deviations σ_τ are pointed out. The dephasing times of a few coherences could not be extracted with a reliable experimental error due to the limited resolution. Dephasing times were obtained by fitting complex oscillatory signals in the time domain (for details, see the Supplementary Text online).

$\omega_2 \text{ (cm}^{-1}\text{)}$	Dephasing time (fs)	σ_τ (fs)	Origin of coherence
± 80	$\gtrsim 500$	–	Electronic $ S_3\rangle\langle S_4 $
± 180	–	–	Vibrational
± 235	360	160	Mixed $ S_4^*\rangle\langle S_5 $
± 307	280	130	Electronic $ S_2\rangle\langle S_4 $
± 380	> 600	–	Vibrational
± 450	–	–	Vibrational
± 570	80	20	Electronic $ S_5\rangle\langle S_6 $
± 615	200	30	Electronic $ S_4\rangle\langle S_5 $
± 695	190	40	Electronic $ S_3\rangle\langle S_5 $

ground or the other (for example, triplet) state (for more details see the Supplementary Text online).

Coherent beatings in the 2D spectra can be conveniently visualised by applying Fourier transforms $t_2 \rightarrow \omega_2$ to the residuals [24, 25]. The resulting Fourier amplitude dependency is a three-dimensional $(\omega_1, \omega_2, \omega_3)$ bulk spectrum, the 2D slices (ω_1, ω_3) , or the so-called oscillation maps, of which can be plotted for a fixed frequency ω_2 . Notice that evolution of Hermitian conjugate coherences $|a\rangle\langle b|$ and $|b\rangle\langle a|$ appears at positive and negative ω_2 frequencies, respectively[26].

The 2D slices at a few selected ω_2 frequencies are shown in Fig. 3A-D. Judging by their pattern, three types of peak configurations can be distinguished. (i) The maps at $\omega_2 = \pm 80, \pm 307, \pm 570, \pm 615, \pm 695$, and $\pm 1150 \text{ cm}^{-1}$ shown in Fig. 3A-B are *diagonally symmetric*, i. e. positive and negative ω_2 features are mirror images of each other with respect to the diagonal as specifically showed in Fig. 3A for $\omega_2 = \pm 80 \text{ cm}^{-1}$. (ii) Oscillation maps at $\omega_2 = +380 \text{ cm}^{-1}$ and -380 cm^{-1} , shown in Fig. 3C, are highly *diagonally asymmetric* with the features below the diagonal in the $\omega_2 = -380 \text{ cm}^{-1}$ map significantly stronger than in the $\omega_2 = +380 \text{ cm}^{-1}$ map. (iii) Features in the $\omega_2 = -235 \text{ cm}^{-1}$ and $\omega_2 = +235 \text{ cm}^{-1}$ maps (Fig. 3D) are *diagonally asymmetric*, but their amplitudes are of the similar magnitude for positive and negative frequency maps. Refer to the Supplementary Fig. S1 for oscillation maps at all other distinguishable frequencies.

We have previously shown that electronic, vibrational, and mixed coherences are, in theory, manifested by their characteristic patterns and symmetries in the coherence maps[3]. The symmetry of the experimental maps at $\omega_2 = \pm 80, \pm 307, \pm 570, \pm 615, \pm 695 \text{ cm}^{-1}$, and $\pm 1150 \text{ cm}^{-1}$ (Fig. 3A and B) indicate that the underlying coherences are of the electronic origin. Dephasing times of these coherences are shorter than 300 fs (Table I), oscillations are present only in the off-diagonal regions in the rephasing 2D spectrum (and only in the

diagonal peaks in the non-rephasing 2D spectrum; see Supplementary Fig. S2), and the peaks at positive and negative ω_2 frequencies are of the same amplitude.

The electronic coherence with $\omega_2 = +80 \text{ cm}^{-1}$ (and $\omega_2 = -80 \text{ cm}^{-1}$) can be assigned to the coherent superposition $|S_4\rangle\langle S_3|$ (and $|S_3\rangle\langle S_4|$) of the closely-positioned electronic states in the vicinity of 11655 cm^{-1} . The electronic coherence at $\omega_2 = \pm 307 \text{ cm}^{-1}$ shows up only in the measurement using laser pulses at 880 nm, signifying electronic quantum beats between states $|S_2\rangle$ and $|S_4\rangle$, that could not be excited by laser pulses at 800 nm.

Beatings with the $\pm 570, \pm 615, \pm 695 \text{ cm}^{-1}$ and $\pm 1150 \text{ cm}^{-1}$ frequencies represent quantum coherences $|S_5\rangle\langle S_6|$, $|S_4\rangle\langle S_5|$, $|S_3\rangle\langle S_5|$ and $|S_4\rangle\langle S_6|$ (and their Hermitian conjugates). We find crosstalk in oscillation maps at $\omega_2 = \pm 570, \pm 615$, and $\pm 695 \text{ cm}^{-1}$ due to the overlapping of different beating frequencies and limited frequency resolution resulting from the damped dynamic coherences. For example, two weaker peaks in the map of $\omega_2 = \pm 615 \text{ cm}^{-1}$ indicate the crosstalk from coherences $|S_4\rangle\langle S_5|$ and $|S_5\rangle\langle S_4|$ with $\pm 570 \text{ cm}^{-1}$ frequency (Fig. 3B). The crosstalk between different frequencies is supported by observation that the weaker peaks are shifted away from the $\omega_3 = \omega_1 \pm 615 \text{ cm}^{-1}$ dashed lines, parallel to the diagonal. Thus, our findings imply that states $|S_1\rangle$ through $|S_6\rangle$ are of electronic origin in contrast to previous assignment[20, 21] (it should be noted that the previously suggested vibrational progression does not follow a displaced harmonic oscillator model).

We assign beatings with the $\omega_2 = \pm 380 \text{ cm}^{-1}$ frequency to the vibrational coherence. This follows from the oscillation maps (Fig. 3C), which have the pattern of oscillating peaks typical for the vibrational coherence[27]: the $\omega_2 = -380 \text{ cm}^{-1}$ map contains many features below the diagonal, while the $\omega_2 = +380 \text{ cm}^{-1}$ map is similar to the electronic coherence maps presented in Fig. 3A and B. In contrast to the electronic coherences, the amplitude of the $\omega_2 = -380 \text{ cm}^{-1}$ map is significantly stronger than that of $\omega_2 = +380 \text{ cm}^{-1}$ [2, 28]. Detailed analysis of the map implies that the vibrational ground state coherences $|g\rangle\langle g^*|$ ($|g^*\rangle$ denotes some vibrationally hot ground state) appear exclusively at $\omega_2 < 0$. Their strong amplitudes are therefore related to the long lifetimes of the ground state vibrations compared with the ones at electronic excited states and mapped onto $\omega_2 = +380 \text{ cm}^{-1}$. Similar maps at $\omega_2 = 180 \text{ cm}^{-1}, 450 \text{ cm}^{-1}$, and 835 cm^{-1} (see the Supplementary Text online) imply their vibrational origin as well.

However, beatings at $\omega_2 = \pm 235 \text{ cm}^{-1}$ point out to the mixed coherence, signifying the superposition state of the $|S_5\rangle$ electronic state and vibronically hot state $|S_4^*\rangle$ (380 cm^{-1} vibrational mode). The corresponding oscillation map is not typical of neither vibrational nor electronic coherences (see Fig. 3D) and the beating frequency 235 cm^{-1} is equal to the difference between the corresponding states.

To support the assignment of the excited states and the natures of the corresponding quantum coherences,

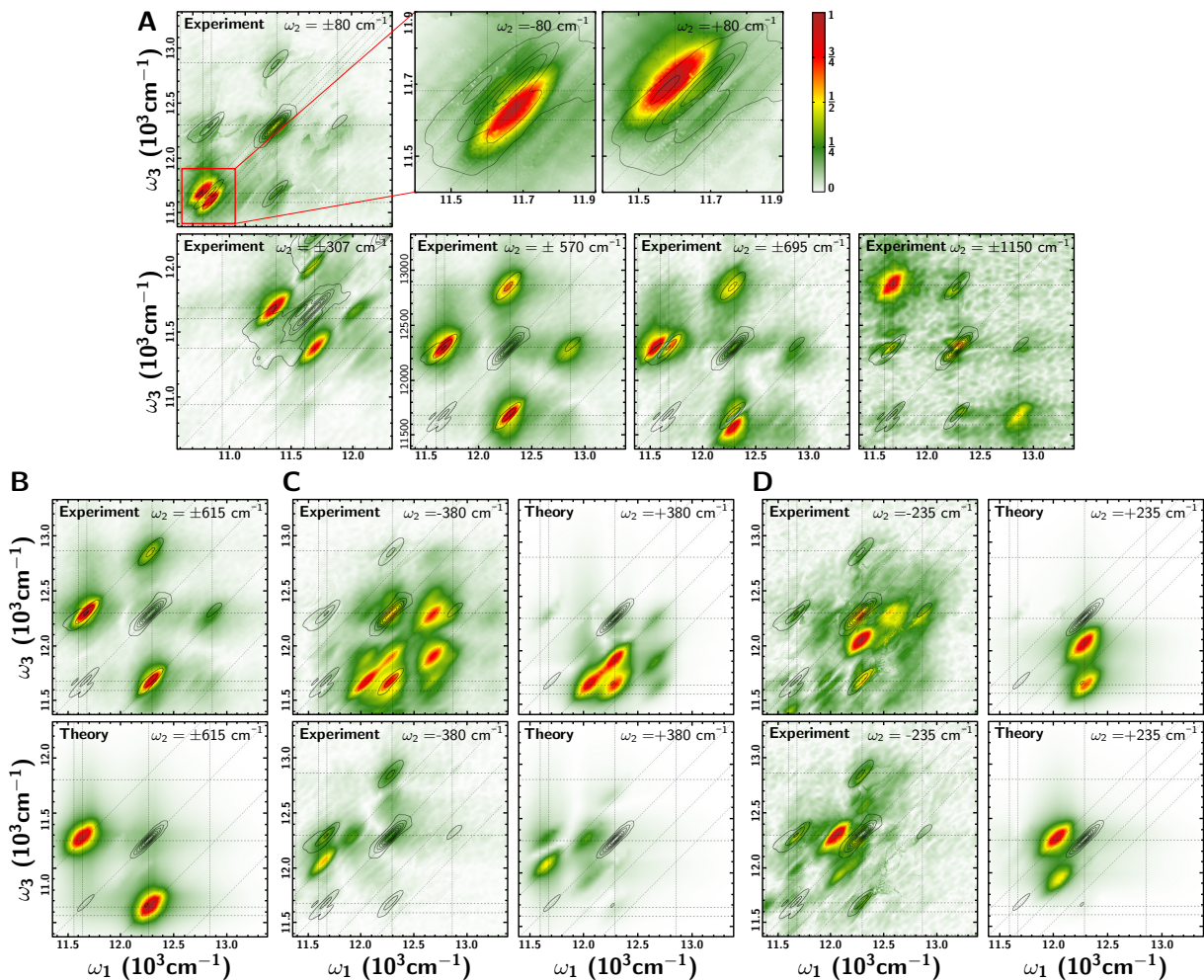


Figure 3. **Diversity of coherences revealed by oscillation maps with different feature patterns.** (A) experimental coherence maps of *electronic* coherences at $\omega_2 = \pm 80, \pm 307, \pm 570, \pm 695, \text{ and } \pm 1150 \text{ cm}^{-1}$; (B) experimental and simulated oscillation maps for *electronic* coherence at $\omega_2 = \pm 615 \text{ cm}^{-1}$; (C) *vibrational* coherence at $\omega_2 = \pm 380 \text{ cm}^{-1}$; (D) *mixed vibronic* coherence at $\omega_2 = \pm 235 \text{ cm}^{-1}$. Intensity of oscillations at each point of a map is indicated by the colour scale; background contours show 2D rephasing spectrum at waiting time 30 fs. Each experimental and simulated map for particular frequency is independently normalized to the maximal amplitude of either positive or negative frequency map. Dashed lines parallel to the diagonal are separated by the value of ω_2 . Dashed vertical and horizontal lines indicate the energies of transitions to electronic states S_1 through S_6 .

two different theoretical models were considered: the *electronic-only* model of six excitonically coupled porphyrin molecules and the *vibronically coupled* dimer model. The electronic-only model is used to capture the connection between the cyclic symmetry of the system and its optical response. The vibronic model supports assignment of the vibrational, electronic, and mixed features.

In the electronic-only model, the nanoring is represented by six two-level sites, representing porphyrins in a circular arrangement, each site characterized by a single transition dipole, rotated by an angle $\alpha = 49^\circ$ with respect to the tangent of the nanoring backbone. Two types of deformations—twisting and bending of the ring backbone—were taken into consideration (refer to the inset in Fig. 1A). Due to the full π -conjugation of the

nanoring, the interaction between any two porphyrins cannot be described by the dipole-dipole approximation and appropriate scaling factors of the coupling constants calculated in the dipole-dipole approximation for the nearest, next-nearest, and next-next-nearest neighbors were obtained by fitting the electronic-only model to the experimental absorption spectrum (see the Supplementary Text online for more details). The simulated absorption spectrum of this model is presented in Fig. 1B by the red dashed line. The agreement with the experimental absorption spectrum is quite good except of the intensity of the S_5 transition. The absence of vibronic coupling in the electronic-only model may be responsible for this discrepancy. Particularly, the electronic model provides the basis of the observed electronic coherences described above. However, additional vibrational/vibronic ingredi-

ents are necessary to explain the remaining coherences.

For qualitative simulations of the vibronic coupling in the porphyrin nanoring we used the theoretical approach developed for a vibronic molecular dimer[3, 29], extended by including two vibrational modes. We assume that two electronic states with the highest oscillator strengths, S_4 and S_5 , are coupled to two vibrational modes of 380 cm^{-1} and 450 cm^{-1} with the Huang–Rhys factors of 0.03 and 0.01, respectively. This allows to significantly improve the description of the absorption spectrum in the range of S_4 and S_5 peaks (Fig. 1B). We also performed simulations of the 3D spectra and extracted its 2D slices at various ω_2 values, corresponding to electronic, vibrational and mixed coherences (Fig. 3B, C and D). Although we included only two electronic states in the vibronic model, calculated and experimental maps of the vibrational coherences at $\pm 380\text{ cm}^{-1}$, the electronic coherences at $\pm 615\text{ cm}^{-1}$, and the mixed coherences at $\pm 235\text{ cm}^{-1}$ are in a very good agreement with the experimental ones, confirming our assignments.

By this analysis we prove the coexistence of electronic, vibrational and mixed coherences in a single system of the porphyrin hexamer. Analysis of quantum coherences aids in disentangling the energy level structure of the

excited states and their cooperativity. This turns out to manifest even in the absorption spectrum, where we identify electronic transitions, the intensity and positions of which are non-trivially defined by vibronic coupling (together with small ring deformations). In the 3D measurement the whole “zoo” of coherences gets raised and they inter-operate to maintain long coherence lifetimes and coherent excitation evolution. Such coherent quantum properties of a supermolecular system are reported for the first time, but should be general for molecular aggregates.

ACKNOWLEDGMENTS

D. Z. and J. A. were supported by Swedish Research Council, the Knut and Alice Wallenberg Foundation, the Wenner–Gren Foundation, and partially funded by the European Social Fund under the Global grant measure. The work in Oxford was supported by European Commission (Marie Curie Individual Fellowship to P. N. under contract PIEF-GA-2011-301336). V. B. and D. A. acknowledge the support of the European Social Fund under the Global Grant Measure (No. VP1-3.1-ŠMM-07-K-01-020).

-
- [1] H. S. Nalwa, ed., *Handbook of organic conductive molecules and polymers*, Vol. 1–4 (John Wiley & Sons Chichester, 1997).
- [2] V. Tiwari, W. K. Peters, and D. M. Jonas, *Proc. Natl. Acad. Sci. USA* **110**, 1203 (2013).
- [3] V. Butkus, L. Valkunas, and D. Abramavicius, *J. Chem. Phys.* **140**, 034306 (2014).
- [4] G. Engel, T. Calhoun, E. Read, T. Ahn, T. Mančal, Y.-C. Cheng, R. Blankenship, and G. Fleming, *Nature* **446**, 782 (2007).
- [5] E. Collini and G. D. Scholes, *Science* **323**, 369 (2009).
- [6] A. Nemeth, F. Milota, T. Mančal, V. Lukeš, J. Hauer, H. Kauffmann, and J. Sperling, *J. Chem. Phys.* **132**, 184514 (2010).
- [7] D. Hayes, G. B. Griffin, and G. S. Engel, *Science* **340**, 1431 (2013).
- [8] A. Halpin, P. J. M. Johnson, R. Tempelaar, R. S. Murphy, J. Knoester, T. L. C. Jansen, and R. J. D. Miller, *Nature Chem.* **6**, 196 (2014).
- [9] F. D. Fuller, J. Pan, A. Gelzinis, V. Butkus, S. S. Senlik, D. E. Wilcox, C. F. Yocum, L. Valkunas, D. Abramavicius, and J. P. Ogilvie, *Nature Chem.* **6**, 706 (2014).
- [10] E. Romero, R. Augulis, V. I. Novoderezhkin, M. Ferretti, J. Thieme, D. Zigmantas, and R. van Grondelle, *Nature Phys.* **10**, 676 (2014).
- [11] N. Christensson, F. Milota, J. Hauer, J. Sperling, O. Bixner, A. Nemeth, and H. Kauffmann, *J. Phys. Chem. B* **115**, 5383 (2011).
- [12] R. Tempelaar, C. P. van der Vegte, J. Knoester, and T. L. C. Jansen, *J. Chem. Phys.* **138**, 164106 (2013).
- [13] N. Christensson, H. Kauffmann, T. Pullerits, and T. Mančal, *J. Phys. Chem. B* **116**, 7449 (2012).
- [14] A. W. Chin, J. Prior, R. Rosenbach, F. Caycedo-Soler, S. F. Huelga, and M. B. Plenio, *Nature Phys.* **9**, 113 (2013).
- [15] D. Abramavicius and S. Mukamel, *J. Chem. Phys.* **134**, 174504 (2011).
- [16] G. Panitchayangkoon, D. Voronine, D. Abramavicius, J. Caram, N. Lewis, S. Mukamel, and G. Engel, *Proc. Natl. Acad. Sci. USA* **108**, 20908 (2011).
- [17] H. Dong and G. R. Fleming, *J. Phys. Chem. B* **118**, 8956 (2014).
- [18] J. Womick and A. Moran, *J. Phys. Chem. B* **115**, 1347 (2011).
- [19] A. Kolli, E. O’Reilly, G. Scholes, and A. Olaya-Castro, *J. Chem. Phys.* **137**, 174109 (2012).
- [20] J. K. Sprafke, D. V. Kondratuk, M. Wykes, A. L. Thompson, M. Hoffmann, R. Drevinskis, W.-H. Chen, C. K. Yong, J. Kärnbratt, J. E. Bullock, M. Malfois, M. R. Wasielewski, B. Albinsson, L. M. Herz, D. Zigmantas, D. Beljonne, and H. L. Anderson, *J. Am. Chem. Soc.* **133**, 17262 (2011).
- [21] M. Hoffmann, J. Kärnbratt, M.-H. Chang, L. M. Herz, B. Albinsson, and H. L. Anderson, *Angew. Chem. Int. Ed.* **47**, 4993 (2008).
- [22] T. Brixner, J. Stenger, H. M. Vaswani, M. Cho, R. E. Blankenship, and G. R. Fleming, *Nature* **434**, 625 (2005).
- [23] J. Dostál, F. Vácha, J. Pšenčík, and D. Zigmantas, *J. Phys. Chem. Lett.* **5**, 1743 (2014).
- [24] J. Seibt and T. Pullerits, *J. Phys. Chem. C* **117**, 18728 (2013).
- [25] F. V. A. Camargo, H. L. Anderson, S. R. Meech, and I. A. Heisler, *J. Phys. Chem. A* **0**, null (0).

- [26] H. Li, A. D. Bristow, M. E. Siemens, G. Moody, and S. T. Cundiff, *Nature Commun.* **4**, 1390 (2013).
- [27] V. Butkus, D. Zigmantas, L. Valkunas, and D. Abramavicius, *Chem. Phys. Lett.* **545**, 40 (2012).
- [28] V. Butkus, D. Zigmantas, D. Abramavicius, and L. Valkunas, *Chem. Phys. Lett.* **587**, 93 (2013).
- [29] E. Bašinskaitė, V. Butkus, D. Abramavicius, and L. Valkunas, *Photosynth. Res.* **121**, 95 (2014).